ADVANCED MATERIALS
www.advmat.de

Inhalable Nanovaccine Based on Bioengineered Bacteria-Derived Membrane Vesicles Against Lung Metastasis

*Yu Miao, Hanlin Zhang, Cheng Wang, Pengxing Li, Linfu Chen, Zheyu Kang, Zhisheng Xiao, Qiang Zhang, Zhiqiang Wu, Yang Yang, and Qian Chen**

Lung metastases pose a challenge in cancer treatment due to the lung's vascular network and immunosuppressive microenvironment. Conventional subcutaneous vaccines typically fail to elicit localized immune responses at metastatic sites. To address this, an inhalable nanovaccine, BMVax (bacterial membrane-based vaccine), is developed using bacterial membrane vesicles from engineered *E. coli* expressing ClyA-OVA$_{257\text{-}264}$. Proteomics with retention of immunostimulatory membrane proteins, enabled efficient antigen co-delivery. BMVax ensured antigen cross-presentation (2.2-fold increase compared to the antigen + BMV mixture), driving robust antigen-specific T-cell proliferation. Inhaling triggers strong immune responses in tracheobronchial lymph nodes, boosting germinal center B cells (≈5.8-fold), follicular helper T cells (≈4.9-fold), and mature dendritic cells (≈2.5-fold), achieving 83.3% complete prevention of lung metastasis. In B16-OVA lung metastasis model, inhaled BMVax demonstrates superior tumor suppression compared to subcutaneous administration. It induces doubling germinal center B cells and 2.9-fold more follicular helper T cells in the lymph nodes, as well as 2.9-fold more antigen-specific T cells in lung tissue than subcutaneous immunization. Tumor-infiltrating T cells exhibit enhanced cytotoxicity and proliferation, reinforcing its therapeutic advantage over subcutaneous immunization. These findings highlight BMVax's potential as an inhalable cancer vaccine, capable of inducing strong immune responses, to effectively combat lung metastatic malignancies.

1. Introduction

Given the extensive vascularization and immune-permissive microenvironment of the lungs, they are a primary site for metastatic dissemination in various cancers.[1,2] Currently, surgical resection remains the predominant treatment for most cancers, with chemotherapy commonly used as an adjunctive therapy to mitigate post-surgical metastasis.[3] However, the clinical effectiveness of chemotherapy is often compromised by systemic toxicity, immunosuppressive side effects, and the development of drug resistance.[4,5] In light of these, there has been a growing shift toward alternative strategies that offer more precise targeting of metastatic cells, with minimal collateral damage to healthy tissue.[6] Among these, cancer vaccines have emerged as a promising approach, gaining significant attention in recent years for their potential to elicit robust, antigen-specific immune responses.[7–9] However, conventional cancer vaccines face several inherent challenges, including suboptimal antigen delivery efficiency, insufficient immune activation, and difficulties with adjuvant selection, all of which contribute to inconsistent immune responses.[10–12] In clinical practice, most vaccines are administered via subcutaneous or intramuscular injection, resulting in limited ability to induce robust local immune responses at mucosal sites such as the respiratory tract.[13,14] This limitation hampers the activation of the local immune microenvironment, which is essential for establishing durable immune memory and effective defense against tumors.[15–17] Therefore, it is essential to overcome these limitations by optimizing antigen delivery, enhancing immune activation, and improving the ability to generate durable and localized immune responses, particularly in lung tissues relevant to tumor metastasis.

Inhalable mucosal vaccines present a promising alternative by directly delivering vaccines to the lungs, the primary site for metastatic cell colonization.[18,19] Unlike traditional subcutaneous vaccines that primarily induce systemic immunity, mucosal vaccines leverage the lungs' extensive immune

Y. Miao, H. Zhang, C. Wang, P. Li, L. Chen, Z. Kang, Z. Xiao, Q. Chen
Institute of Functional Nano & Soft Materials (FUNSOM)
Jiangsu Key Laboratory for Carbon-Based Functional Materials & Devices
Soochow University
Suzhou 215123, China
E-mail: chenqian@suda.edu.cn
Q. Zhang, Z. Wu, Y. Yang
School of Materials Science and Engineering
Tongji University
Shanghai 201804, China
Z. Wu, Y. Yang
Department of Thoracic Surgery
Shanghai Pulmonary Hospital
School of Medicine
Tongji University
Shanghai 200433, China
The ORCID identification number(s) for the author(s) of this article can be found under https://doi.org/10.1002/adma.202506174

DOI: 10.1002/adma.202506174

network to trigger strong localized responses right at the invasion site.[20–22] By directly engaging lung-resident antigen-presenting cells, inhaled vaccines enhance antigen uptake, promote efficient antigen presentation, and provoke robust mucosal immune responses.[23] Furthermore, mucosal vaccination not only elicits potent local immune activation but also facilitates the development of systemic immune memory, ensuring long-term pathogen surveillance.[8,13] Nevertheless, significant challenges remain, particularly in ensuring the effective antigen penetration across the mucosal barrier—a critical step for achieving optimal antigen presentation and immune activation.[24,25] For an efficient inhalation vaccine, optimizing antigen stability, enhancing antigen presentation, and ensuring efficient uptake by lung-resident antigen-presenting cells are crucial.[23,26] Therefore, achieving deep lung deposition and overcoming the mucosal barrier for inhalable vaccines are essential to maximizing immune responses.

Bacterial membrane vesicles (BMVs), derived from bacterial lysis, which are nanoscale structures that retain critical immunostimulatory components, such as lipopolysaccharides and porins, are emerging as an innovative platform for cancer vaccines.[27–29] In addition to their innate immunostimulatory properties, BMVs can be genetically engineered to incorporate specific antigens, positioning them as a dual-functional tool that serves both as an antigen and an endogenous adjuvants.[30,31] This ability to synchronize spatial and temporal immune stimulation offers a significant advantage over traditional live bacteria or synthetic nanoparticles, which often struggle to achieve such precise coordination.[17,32,33] Notably, recent research has demonstrated that BMVs possess intrinsic permeation capabilities that enable them to efficiently penetrate mucosal barriers—a critical requirement for inhalable vaccines aimed at targeting the lungs.[24,34–36] Therefore, the powerful editability and mucosal barrier penetration capabilities of BMVs, coupled with their robust immune activation, position them as a promising strategy to develop inhalable mucosal vaccines targeting lung metastasis.

Herein, we present an innovative inhalable vaccine system based on engineered bacterial membrane vesicles (BMVax), as illustrated in **Scheme 1**. The $OVA_{257-264}$ antigen was encoded into a pBAD-ClyA-OVA plasmid and transfected into *Escherichia coli TOP10* (*E. coli*-$OVA_{257-264}$), allowing the expression of $OVA_{257-264}$ antigen on the bacterial membrane surface. Membrane vesicles were then isolated through a combination of ultrasonication, freeze-thaw cycles, and high-speed centrifugation.[8,37,38] The resulting BMVax preserved both immunostimulatory properties and the $OVA_{257-264}$ antigen, displaying a uniform nanoscale size and exceptional stability. In vitro studies demonstrated that BMVax significantly enhanced antigen internalization and cross-presentation, effectively inducing antigen-specific T cell immune responses. Inhalation immunization with BMVax activated germinal center (GC) B cells, mature dendritic cells (DCs), and follicular helper T (Tfh) cells in the tracheobronchial lymph nodes (TBLNs), with increases of 5.8-fold, 2.5-fold, and 4.9-fold, respectively. Additionally, there was a substantial rise in tissue-resident $CD8^+$ T cells and antigen-specific $CD8^+$ T cells in lung tissues, with increases of 3.9-fold and 2.7-fold, respectively. Remarkably, these localized immune responses also induced systemic immune activation, with $CD8^+$ T cells in the spleen exhibiting elevated levels of tumor necrosis factor-α (TNF-α) and interferon-γ (IFN-γ) upon antigen restimulation. In a melanoma B16-OVA lung metastasis model, BMVax demonstrated significant anti-metastatic effects, achieving an 83.3% complete prevention rate of lung metastases, with only 1 out of 6 immunized mice exhibiting mild signs of melanoma lung metastasis 30 days post tumor inoculation. More interestingly, compared to subcutaneous administration, inhaled BMVax significantly enhanced germinal center B cells (2-fold) and Tfh cells (2.9-fold) in lymph nodes, as well as antigen-specific T cells (2.9-fold) in lung tissue. Moreover, tumor-infiltrating T cells exhibited superior cytotoxicity and proliferative capacity. In contrast, while subcutaneous immunization increased tumor-infiltrating T cells, it failed to activate immune responses in the tracheobronchial lymph nodes or enhance antigen-specific T-cell recruitment in the lungs, resulting in diminished therapeutic efficacy, as evidenced by the presence of substantial pulmonary tumor nodules. Inhalation immunization, however, led to a marked reduction in tumor burden, with only minimal residual nodules observed, indicating a near-complete therapeutic response. The straightforward and efficient production process, coupled with excellent antigen delivery efficiency and potent preventive and therapeutic effects against lung metastases, highlights the potential of using membrane vesicles derived from engineered bacteria for developing an inhalable cancer vaccine, which should be a groundbreaking strategy in cancer immunotherapy.

2. Results and Discussion

2.1. Preparation and Characterization of BMVax

To engineer the bacteria, we initially designed the plasmid pBAD-ClyA-OVA, incorporating essential functional elements, including the ampicillin resistance gene (AmpR), an origin of replication (Ori), a mob site for plasmid mobilization, the arabinose operon regulatory gene (araC), and the arabinose-inducible araBAD promoter (pBAD), which enables precise expression control in response to L-arabinose. The plasmid encodes a gene fusion of ClyA and the antigenic peptide $OVA_{257–264}$, with ClyA serving as a membrane-anchoring domain to promote the surface display of the fused antigen. This plasmid was introduced into *Escherichia coli TOP10* (*E. coli*) by electroporation to enable arabinose-inducible surface expression of the $OVA_{257-264}$ peptide (**Figure 1a,b**). To obtain BMVs, the bacteria were first obtained via centrifugation and then subjected to sonication to disrupt the membrane and release intracellular components. Subsequently, freeze-thaw cycles with liquid nitrogen were applied to further promote membrane rupture and increase the yield of membrane vesicles. Ultracentrifugation was then employed to separate and collect the vesicles, resulting in two types: non-engineered BMV and engineered BMVax. The production yield of BMVax, quantified by measuring the total protein content extracted from the culture supernatant, achieved 12.33% ± 2.18%, indicating its potential for high-yield and scalable manufacturing.

To verify the successful expression of ClyA-$OVA_{257-264}$ in *E. coli*-$OVA_{257-264}$ and BMVax, western blot analysis was carried out. As shown in Figure 1c, a band corresponding to ClyA-$OVA_{257-264}$ at ≈35 kDa was clearly visible in both *E. coli*-$OVA_{257-264}$ and BMVax incubated with the inductive agent L-arabinose, while no such band was observed in samples without L-arabinose

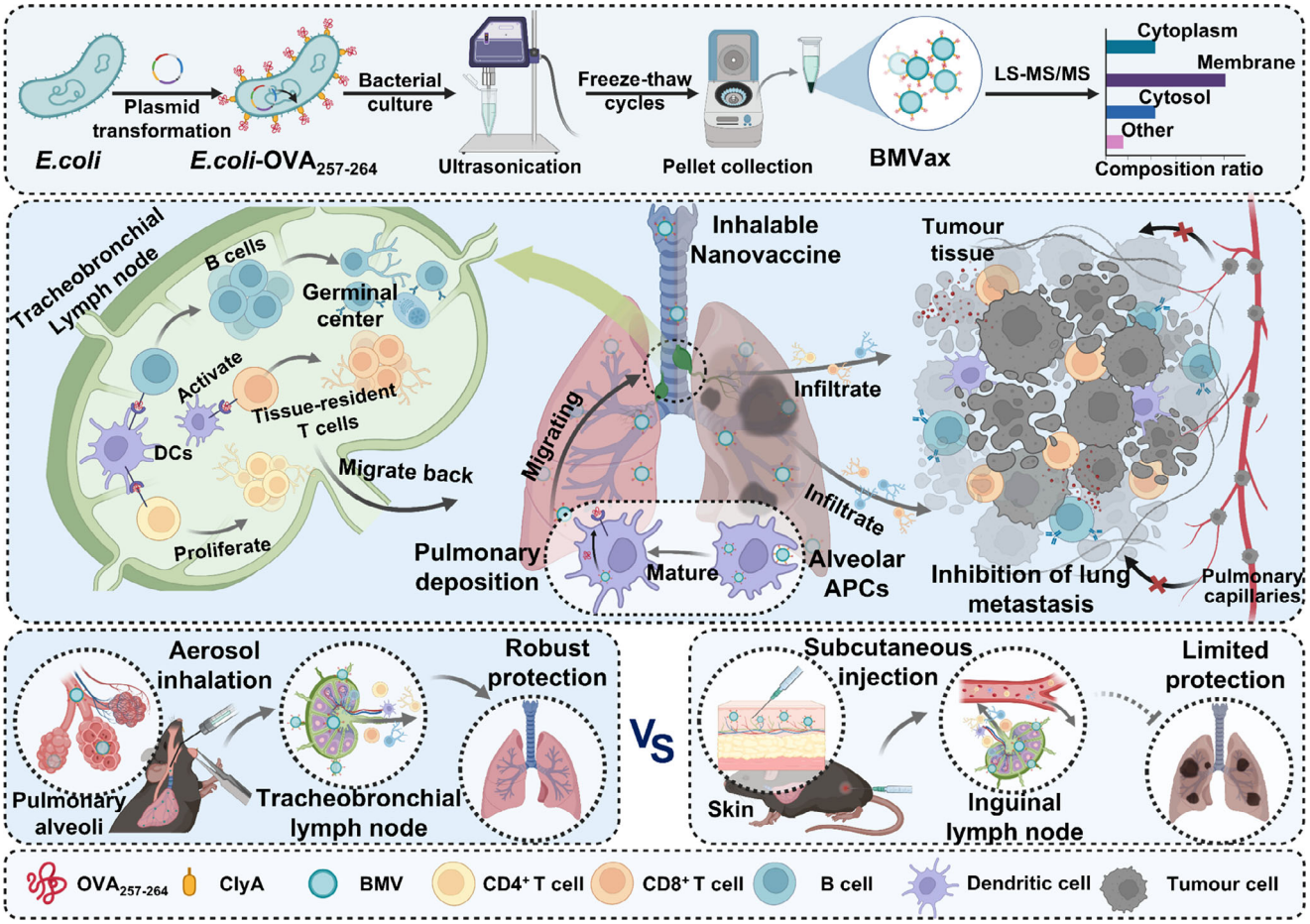

Scheme 1. Schematic illustration of the inhalable nanovaccine leveraging bioengineered bacteria-derived membrane vesicles against lung metastasis. Through genetic engineering, the model antigen $OVA_{257-264}$ was expressed in bacteria and presented on their membranes. Bacterial membrane vesicles were then extracted from these engineered bacteria to construct an inhalable nanovaccine (BMVax). Upon direct lung delivery, BMVax is efficiently internalized by antigen-presenting cells (APCs) in the alveoli, which then migrate to the tracheobronchial lymph nodes (TBLNs) to initiate antigen-specific T and B cell responses. This process catalyzes robust germinal center (GC) reactions, thereby enhancing mucosal immunity. Compared to subcutaneous vaccination, direct lung delivery of BMVax induces superior recruitment of antigen-specific T cells to the lung and promotes the formation of tissue-resident memory T cells, ensuring sustained immune surveillance. Consequently, direct lung delivery of BMVax provided significant protection against lung metastasis, highlighting its potential as an effective and advantageous vaccine. All illustrations created in BioRender. Chen, Q. (2025) https://BioRender.com/mu6y6rc.

induction or in non-engineered *E. coli* and BMV, indicating the successful expression of the fusion protein and its corresponding membrane vesicles. Zeta potential analysis revealed that *E. coli* expressing ClyA-$OVA_{257-264}$ exhibited increased surface electronegativity compared to non-transfected bacteria (Figure S1, Supporting Information). Consequently, BMVax demonstrated a slightly more negative charge than BMV (Figure 1d), which may be attributed to the incorporation of ClyA-$OVA_{257-264}$. Both BMVax and BMV exhibited similar and uniform hydrodynamic sizes (Figure 1e), which was confirmed by transmission electron microscopy (TEM) images in Figure 1f, showing their nanometer-scale size and intact membrane structure. Moreover, both BMV and BMVax maintained stable nanoscale sizes at physiological situation (1×PBS, 37 °C) for up to 7 days, with a consistently low polydispersity index (PDI) of less than 0.3 (Figure 1g). Furthermore, BMVax preserved its original particle size and PDI after lyophilization with 5% (w/v) trehalose, supporting its suitability for long-term storage and potential for clinical application (Figure S2, Supporting Information). Moreover, the liquid chromatography–mass spectrometry (LC-MS/MS) analysis revealed that BMVax, derived from *E. coli*-$OVA_{257-264}$, retains a distinct subproteome, which is characterized by a pronounced enrichment of membrane-associated proteins and a concomitant reduction in cytoplasmic and cytosolic components, confirming both the successful plasmid expression and the efficient isolation of membrane vesicles (Figure 1h; Figure S3, Supporting Information). When comparing BMVax to BMV derived from wild-type *E. coli*, we observed a largely similar distribution of protein origins across cytoplasm, cytosolic, plasma membrane, and membrane categories in both vesicle types. Importantly, both BMV and BMVax preserved essential outer membrane proteins known to function as pattern recognition receptor (PRR) agonists, such as OmpA, OmpC, OmpF, OmpX, Pal, TolB, and Lpp, although the relative abundance of these PRR-related proteins

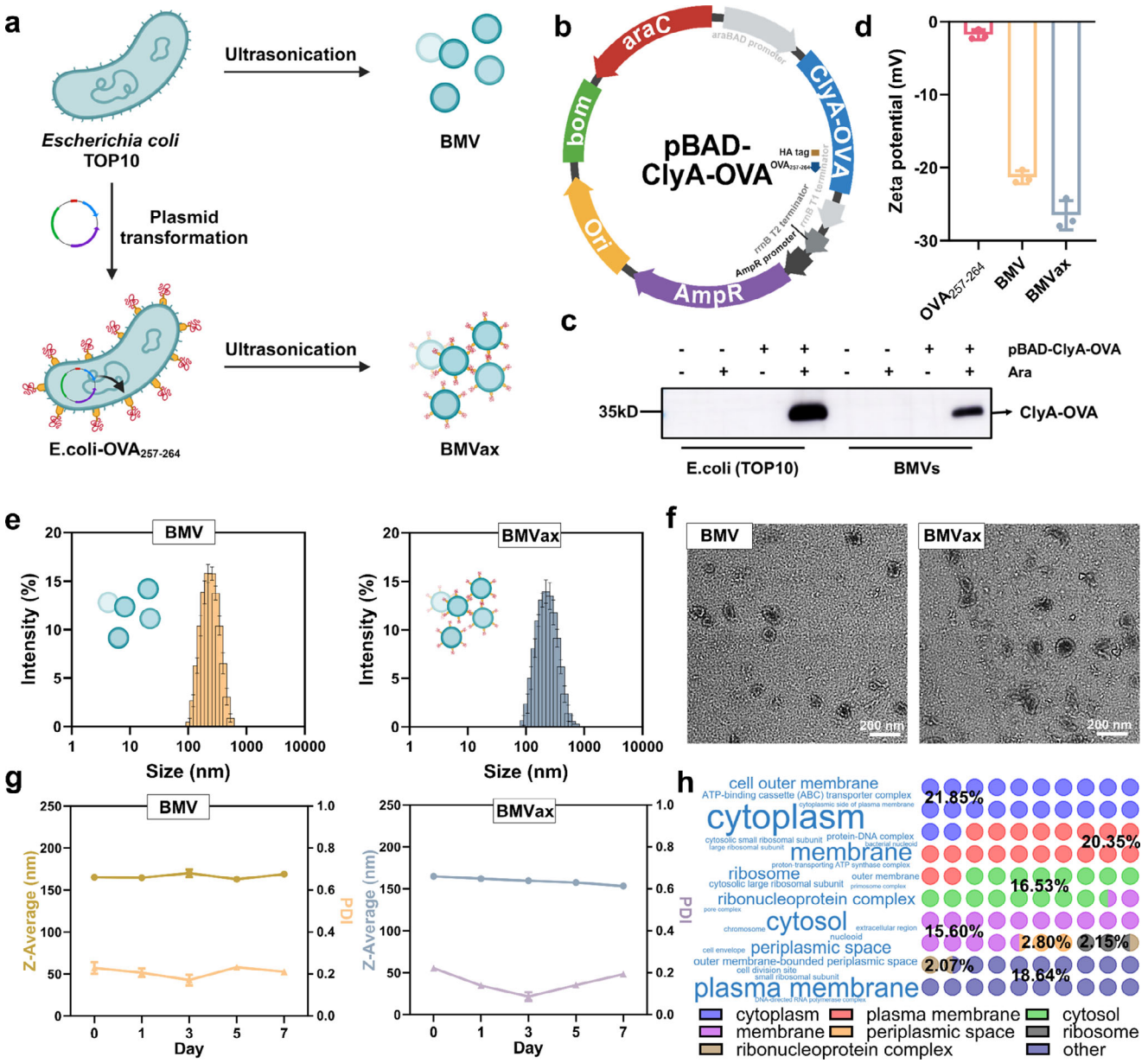

Figure 1. Preparation and characterization of BMVax. a) Schematic illustration showing the preparation of BMV and BMVax. b) Genetic structure of pBAD-ClyA-OVA plasmid. c) Western blot analysis of ClyA-OVA fusion protein expression using anti-HA antibody. d) Zeta potential of $OVA_{257-264}$, BMV, and BMVax in PBS. e) Particle size distributions of BMV and BMVax in PBS. f) TEM images of BMV and BMVax. g) Z-average sizes and PDI of BMV and BMVax in PBS at different time points. h) Number of distinct protein species identified in BMVax using LC-MS/MS. Data are presented as the mean ± SEM ($n = 3$).

was slightly higher in BMV. Collectively, these findings demonstrate that the vesicle preparation process selectively enriches immunologically active membrane components while maintaining a consistent subcellular proteomic profile between BMV and BMVax.

2.2. Biocompatibility and Immune Stimulation of BMVax

Before evaluating the immune-stimulatory potential of BMVax, we first examined its biocompatibility. Both types of membrane vesicles were quantified using the bicinchoninic acid (BCA) assay to ensure consistency in protein concentration. DC2.4 cells and MLE12 cells were incubated with various concentrations of BMV and BMVax for 24 h, after which cell viability was assessed using the standard 3-(4,5-dimethylthiazol-2-yl)-2,5-diphenyltetrazolium bromide (MTT) assay (**Figure** 2a; Figure S4, Supporting Information). Under comparable protein concentrations, BMVax exhibited slightly higher biocompatibility compared to BMV. To explore this difference, we quantified endotoxin levels and found that BMV contained 555.3 EU/250 μg protein, whereas BMVax contained 215.7 EU/250 μg, indicating a

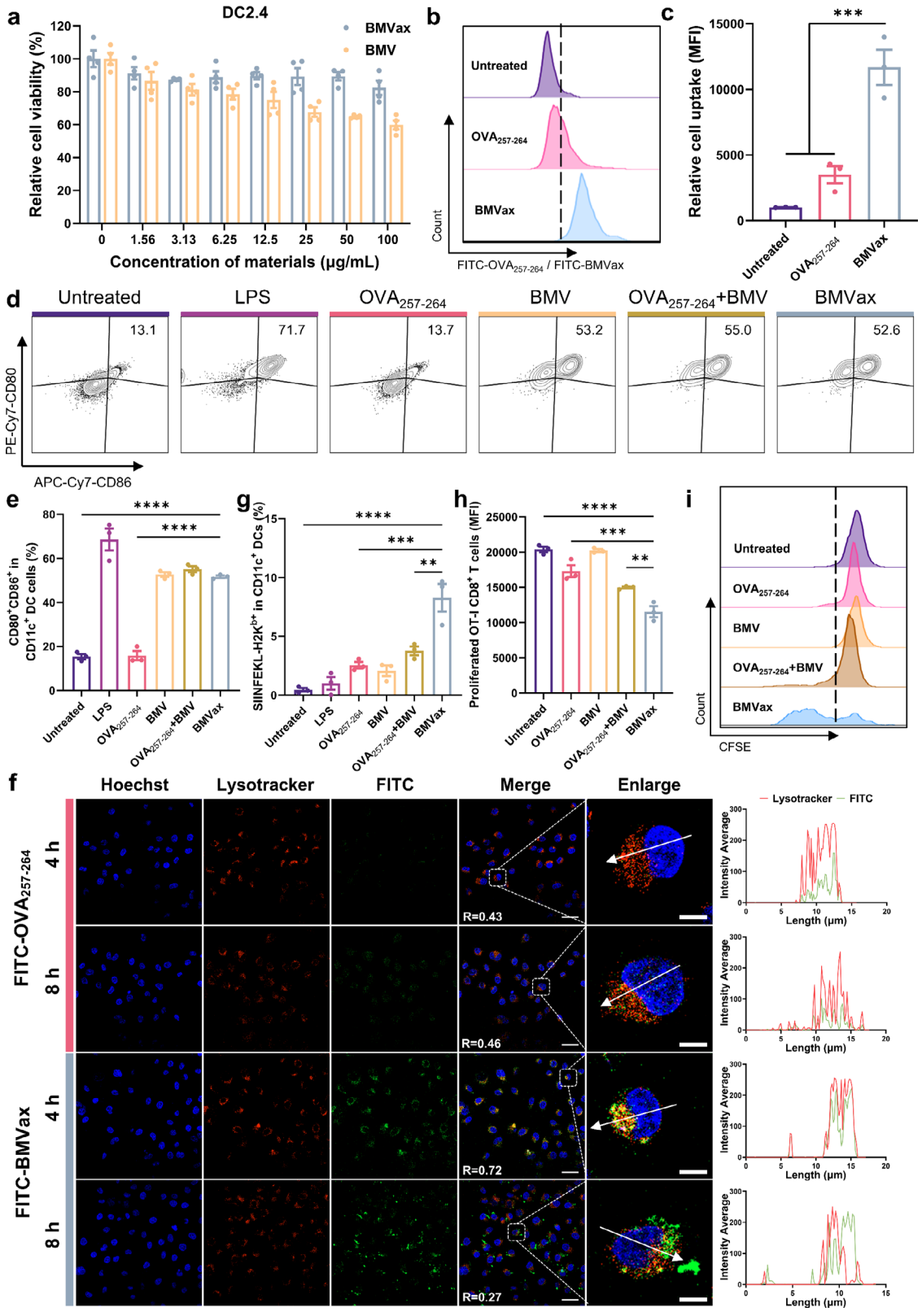

substantial reduction in endotoxin content (Figure S5, Supporting Information). This reduction is likely due to the incorporation of the engineered fusion protein (ClyA-$OVA_{257-264}$) in BMVax, which may reduce the relative proportion of pro-inflammatory components, such as lipopolysaccharides (LPS) or other immunogenic molecules typically present in bacterial membrane vesicles. Therefore, BMVax exhibited enhanced biocompatibility, prompting us to select a concentration of 5 μg mL^{-1}, deemed safe for both BMV and BMVax, for subsequent cellular immune activation experiments.

To investigate the efficiency of BMVax in promoting the internalization of antigen-presenting cells (APCs), we labeled BMVax with FITC and used commercially available FITC-$OVA_{257-264}$ as the free antigen, maintaining equivalent fluorescence intensity for both. They were incubated with DC2.4 cells for 6 h, followed by flow cytometry analysis to analyze the degree of internalization (Figure 2b,c). In addition, cellular fluorescence imaging under the same incubation conditions (Figure S6, Supporting Information) confirmed that BMVax exhibited substantially higher internalization efficiency than the free antigen group. These findings collectively demonstrate that BMVax exhibits significantly higher internalization efficiency than the free antigen, underscoring its potential as an efficient vaccine for enhancing antigen internalization by APCs. Then, we investigated whether BMVax retained its inherent immune stimulating capability. Bone-marrow-derived dendritic cells (BMDCs) were incubated with LPS (1 μg mL^{-1}), Free $OVA_{257-264}$, BMV, $OVA_{257-264}$ + BMV, and BMVax (with equal $OVA_{257-264}$ at 5 μg mL^{-1} and BMV protein concentration at 5 μg mL^{-1}) for 24 h, and the maturation of BMDCs was analyzed by flow cytometry. Remarkably, all groups incubated with vesicles, including BMV, $OVA_{257-264}$ + BMV, and BMVax, exhibited significantly enhanced BMDC maturation compared with the Untreated and Free $OVA_{257-264}$ groups (Figure 2d,e). Meanwhile, the secretion of various pro-inflammatory cytokines, including TNF-α, interleukin-1β (IL-1β), and interleukin-6 (IL-6), was measured. Consistent with the maturation of BMDCs, the cells incubated with BMV or BMVax secreted remarkably elevated levels of TNF-α, IL-1β, and IL-6 (Figure S7, Supporting Information). To further investigate the immune activation potential of BMVax, we evaluated the expression of key immune signaling markers. Both qPCR and western blot analyses indicated upregulation of TLR4 and NF-κB p65 following BMVax stimulation, suggesting activation of innate immune pathways (Figure S8, Supporting Information). Notably, fluorescence staining demonstrated enhanced major histocompatibility complex class I (MHC-I) antigen presentation, as evidenced by increased surface expression of SIINFEKL-$H2K^b$ complexes after BMVax treatment (Figure S9, Supporting Information). These results confirm that BMVax effectively promotes antigen presentation and dendritic cell activation in vitro.

To investigate the internalization dynamics of nanoparticles in antigen delivery, we employed confocal microscopy. DC2.4 cells were cultured with either free FITC-$OVA_{257-264}$ (5 μg mL^{-1}) or FITC-BMVax (5 μg mL^{-1}) in glass bottom cell culture dishes, followed by nuclear and lysosomal staining. As exhibited in Figure 2f, FITC-BMVax exhibited complete colocalization with lysosomes at 4 h. However, by 8 h, the degree of colocalization decreased, suggesting the release of the protein from the lysosomes. In contrast, free FITC-$OVA_{257-264}$ still showed partial colocalization with lysosomes and exhibited a lower FITC signal intensity. Considering that following the release of antigens from the lysosome, DCs would process and present the antigens on their surface, we further analyzed the percentage of $SIINFEKL^+CD11c^+$DCs through flow cytometry. BMDCs were co-incubated with LPS (1 μg mL^{-1}), Free $OVA_{257-264}$, BMV, $OVA_{257-264}$ + BMV, or BMVax (with equal $OVA_{257-264}$ at 5 μg mL^{-1} and BMV protein concentration at 5 μg mL^{-1}) for 24 h, and the extent of antigen cross-presentation was assessed. As shown in Figure 2g, the surface expression of SIINFEKL peptide on BMDCs co-incubated with the BMVax was significantly higher than in the free $OVA_{257-264}$ group and the $OVA_{257-264}$ + BMV group, indicating that the surface expression of the fusion protein on the BMVax vesicles led to more efficient cross-presentation, ≈2.2 times higher than simple co-delivery.

Building on the remarkable efficiency of antigen cross-presentation, we further investigated the ability of DCs to activate antigen-specific T cells in vitro. BMDCs were first primed with Free $OVA_{257-264}$, BMV, $OVA_{257-264}$ + BMV, and BMVax (with equal $OVA_{257-264}$ at 5 μg mL^{-1} and BMV protein concentration at 5 μg mL^{-1}) for 24 h, and then co-incubated with carboxyfluorescein diacetate succinimidyl ester (CFSE) pre-labeled spleen-derived T cells from OT-I mice for an additional 72 h. Analysis of CFSE fluorescence intensity revealed that BMDCs pre-treated with BMVax significantly enhanced the proliferation and differentiation of antigen-specific T cells in vitro compared to BMDCs pre-treated with free $OVA_{257-264}$ and the untreated group (Figure 2h,i). Interestingly, BMDCs primed with $OVA_{257-264}$ + BMV also elicited moderate T cell proliferation, consistent with the known immunostimulatory properties of BMV in promoting DC maturation. However, under the 72-h co-culture conditions, this response was weaker than that induced by BMVax-primed BMDCs, further supporting BMVax's superior efficiency in driving rapid antigen-specific T cell expansion. Furthermore, BMDCs pre-treated with BMVax markedly enhanced the secretion of TNF-α and IFN-γ by OT-I $CD8^+$ T cells (Figure S10, Supporting Information), underscoring their superior potential for activating antigen-specific T cell responses. In conclusion, the engineered bacterial membrane vesicles (BMVax) prepared in this study, with surface-displayed antigens, retained the potent immunostimulatory capabilities inherent to bacterial

Figure 2. In vitro immune activation of BMVax. a) Relative viabilities of DC2.4 after 24-h incubation with BMV and BMVax at different concentrations. b,c) Representative flow cytometry diagram (b) and statistical data (c) showing the FITC signals of DC2.4 cells after different treatments. d,e) Representative flow cytometry diagram (d) and statistical data (e) showing the percentages of $CD86^+CD80^+$ BMDCs after different treatments for 24 h. f) CLSM images of DC2.4 cells treated with FITC-$OVA_{257-264}$ or FITC-BMVax for 4 and 8 h at 37 °C. The cell nuclei and lysosomes were stained with Hoechst (blue) and LysoTracker red (red), respectively. Low- and high-magnification images scale bars were 20 μm and 5 μm. R represents Pearson's R value. The fluorescence intensity statistics on the far right show the red and green signal per unit length of a single cell. g) Percentage of BMDCs presenting SIINFEKL-$H2K^b$ after different treatments for 24 h. h,i) Statistical analysis (h) and representative flow cytometry diagram (i) showing the proliferation of CFSE-staining OT-I $CD8^+$ T cells after 72 h co-culture with BMDCs that had been pre-treated for 24 h. Data are presented as the mean ± SEM ($n = 3$). Statistical significance was calculated via one-way ANOVA in GraphPad Prism. * $p < 0.05$, ** $p < 0.01$, *** $p < 0.001$, and **** $p < 0.0001$.

vesicles. Moreover, BMVax demonstrated superior antigen-specific immune activation compared to the co-delivery of vesicles and antigens. These findings establish a solid foundation for further in vivo investigations to enhance cellular immunity activation.

2.3. Immune Evaluation and Prophylactic Effect of Inhalable BMVax Nanovaccine

Given the remarkable immune-stimulatory properties and antigen presentation efficiency of BMVax in vitro, we aimed to evaluate its immunogenic potential through in vivo immunization. To this end, mice were administered via direct lung delivery to simulate inhalation immunization (40 µL PBS volume), once a week for three consecutive weeks with: Free $OVA_{257-264}$ (10 µg per mouse), BMV (30 µg per mouse), $OVA_{257-264}$ + BMV (10 µg $OVA_{257-264}$ + 30 µg BMV per mouse), and BMVax (30 µg per mouse). Considering the critical role of mucosa-associated lymphoid tissues (MALT) in initiating immune responses,[39,40] particularly in lymph nodes adjacent to mucosal surfaces, we focused on the TBLNs, where germinal center reactions are initiated to mediate mucosal immunity, as well as the activation of DCs and Tfh cells, key players in orchestrating immune responses at mucosal sites.[41–43] On day 7 following the final immunization, TBLNs were collected, and immune cell populations were analyzed by flow cytometry, as outlined in the experimental timeline (**Figure 3a**). As depicted in Figure 3b,c, direct lung delivery of BMVax led to the most pronounced expansion of $B220^+$ B cells within TBLNs. Further examination of GC B cells ($CD38^-GL7^+B220^+$ cells) revealed that ≈10% of the total $B220^+$ B cells from BMVs-immunized mice were in the GC stage (Figure 3d,e), which is ≈5-fold and 3-fold higher than that observed in the untreated and free antigen groups, respectively, underscoring the potent immune activation capacity of BMVs. Additionally, CD95 (Fas), a key marker associated with the selective elimination of inefficient or autoreactive B cells within the GC, was also significantly elevated in all BMVs-immunized mice (Figure 3f; Figure S12, Supporting Information), suggesting that BMVs not only promote GC formation but also facilitate the selection of high-affinity B cell clones.

Furthermore, as key regulators of GC responses, Tfh cells play a crucial role in sustaining GC reactions and promoting B cell activation and differentiation.[44] We further analyzed the abundance and activation status of Tfh cells ($CXCR5^+CD4^+CD3^+$) within the TBLNs. As shown in Figure 3g,h, Figures S13 and S14 (Supporting Information), all BMVs significantly promoted $CD4^+$ T cell expansion, with BMVax inducing the highest Tfh cell frequency—4.7-fold and 2.5-fold higher than those observed in the untreated and free antigen groups, respectively. Furthermore, in the BMVax group, the expression of inducible T cell costimulator (ICOS), a crucial molecule for B cell activation and GC maintenance,[45] was significantly upregulated (Figure 3i; Figure S15, Supporting Information). Simultaneously, the expression of programmed cell death protein 1 (PD-1), which regulates GC dynamics to prevent excessive immune activation,[46] was also remarkedly increased (Figure 3j; Figure S16, Supporting Information). Additionally, we assessed the activation and antigen presentation of DCs, which is crucial for the priming of antigen-specific T cell responses.[47] As expected, all BMV-immunized mice exhibited a significant increase in the proliferation and maturation of $CD11c^+$ DCs within the TBLNs (Figure 3k–m; Figure S17, Supporting Information). Notably, BMVax significantly boosted the proportion of SIINFEKL-$H2K^{b+}$ DCs, ≈1.5-fold higher than in the $OVA_{257-264}$ + BMV group, indicating that the membrane-anchored antigen in BMVax facilitated more efficient antigen delivery and presentation (Figure 3n,o). Collectively, these findings demonstrate that BMVax efficiently elicits a potent antigen-specific immune response within the TBLNs, promoting robust GC B cell activation, Tfh differentiation, and DC maturation, thereby establishing a strong foundation for further enhancing in vivo adaptive immunity through mucosal vaccination strategies.

Given the critical role of the TBLN in antigen presentation and T cell priming, we further explored the migration efficiency of activated T cells to lung tissue, assessing their activation status and antigen specificity.[48] Therefore, we analyzed the presence and functional state of T cells in the lung following direct lung immunization. As shown in **Figure 4a,b**, all BMVs-immunized mice exhibited a substantial expansion of $CD3^+$ T cells in the lung, exhibiting approximately a two-fold increase compared to the free antigen group, suggesting that BMVs effectively enhance T cell recruitment. Notably, only mice immunized with BMVax displayed the highest infiltration of antigen-specific T cells, ≈3.7-fold higher than the free antigen group and 2.7-fold higher than the group receiving a combination of antigen and BMVs (Figure 4c,d). To assess the establishment of local immune memory, we examined the population of tissue-resident memory T cells ($CD69^+CD103^+$) and found a significant increase in all BMVs-immunized groups, highlighting their potential role in fostering long-term mucosal immunity (Figure 4e,f; Figures S19 and S20, Supporting Information). Therefore, BMVax not only enhances the recruitment of antigen-specific T cells, but also promotes the formation of tissue-resident memory T cells, thereby establishing a foundation for sustained immune protection. Beyond local immune activation, direct lung immunization with BMVax also facilitated the systemic expansion of antigen-specific T cells, with splenic levels reaching 1.5-fold higher than those in the free antigen group (Figure S22, Supporting Information). Notably, upon antigen restimulation, only splenic $CD8^+$ T cells from BMVax-immunized mice exhibited a robust recall response, producing significantly higher levels of IFN-γ and TNF-α (Figures S23 and S24, Supporting Information). These findings suggest that BMVax not only enhances effective local immune responses but also drives systemic immune activation, reinforcing its potential for long-term immune protection.

To further evaluate whether the immune response induced by BMVax could effectively suppress lung cancer metastasis, we established a B16-OVA lung metastasis model. As shown in Figure 4g, C57BL/6 mice were administered via direct lung delivery to simulate inhalation immunization (40 µL PBS volume) weekly for three weeks with: Free $OVA_{257-264}$ (10 µg per mouse), BMV (30 µg per mouse), $OVA_{257-264}$ + BMV (10 µg $OVA_{257-264}$ + 30 µg BMV per mouse), and BMVax (30 µg per mouse). On day 21, all immunized mice received an intravenous injection of 1×10^6 B16-OVA cells to induce lung metastases. To assess the vaccine's protective efficacy against B16-OVA cancer cells, the mice were sacrificed on day 50, and their lungs were collected for

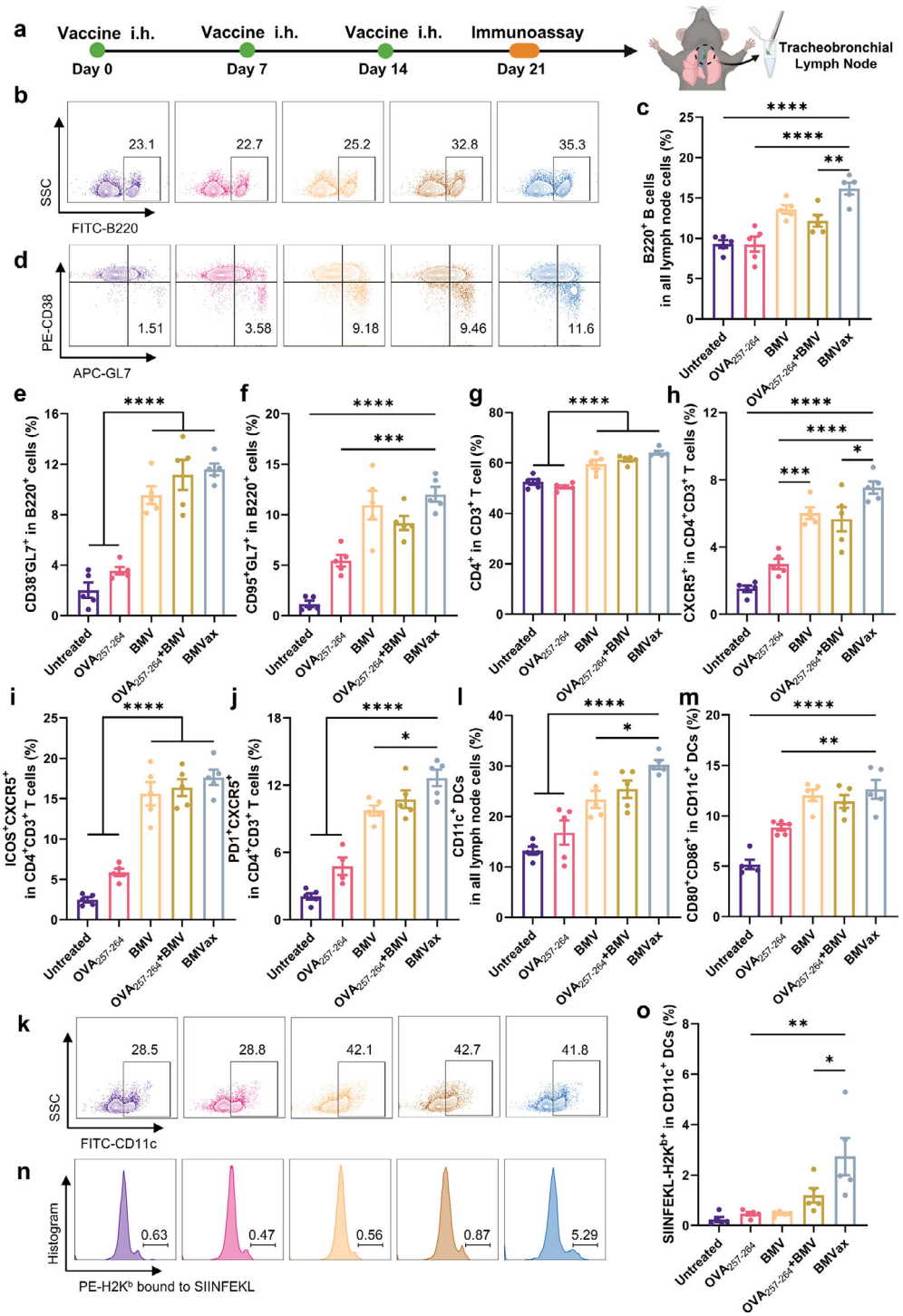

Figure 3. In vivo evaluation of immune responses in tracheobronchial lymph nodes induced by the inhalable BMVax nanovaccine. a) Experimental timeline for evaluating the in vivo immune responses triggered by BMVax nanovaccines. b,c) Representative flow cytometry diagram (b) showing the proportion of $B220^+$ B cells in lymph node single cell suspensions from mice with different treatments and statistical data (c) showing the proportion of $B220^+$ B cells within total lymph node cell populations. d,e) Representative flow cytometry diagram (d) and statistical data (e) showing the proportion of $CD38^-GL7^+$ cells in $B220^+$ cells. f) Statistical data showing the proportion of $CD95^+GL7^+$ cells in $B220^+$ cells. g) Statistical data showing the proportion of $CD4^+$ cells in $CD3^+$ T cells. h) Statistical data showing the proportion of $CXCR5^+$ cells in $CD4^+CD3^+$ T cells. i,j) Statistical data showing the proportion of $ICOS^+CXCR5^+$ cells (i) and $PD1^+CXCR5^+$ cells (j) in $CD4^+CD3^+$ T cells. k–m) Representative flow cytometry diagram (k) showing the proportion of $CD11c^+$ DCs in lymph node single cell suspensions from mice with different treatments and statistical data showing the proportion of $CD11c^+$ DCs within total lymph node cell populations (l) and $CD80^+CD86^+$ cells in DCs (m). n,o) Representative flow cytometry diagram (n) and statistical data (o) showing the proportion of SIINFEKL-$H2K^{b+}$ in $CD11c^+$ DCs. Data are presented as the mean ± SEM ($n = 5$). Statistical significance was calculated via one-way ANOVA in GraphPad Prism. * $p < 0.05$, ** $p < 0.01$, *** $p < 0.001$, and **** $p < 0.0001$.

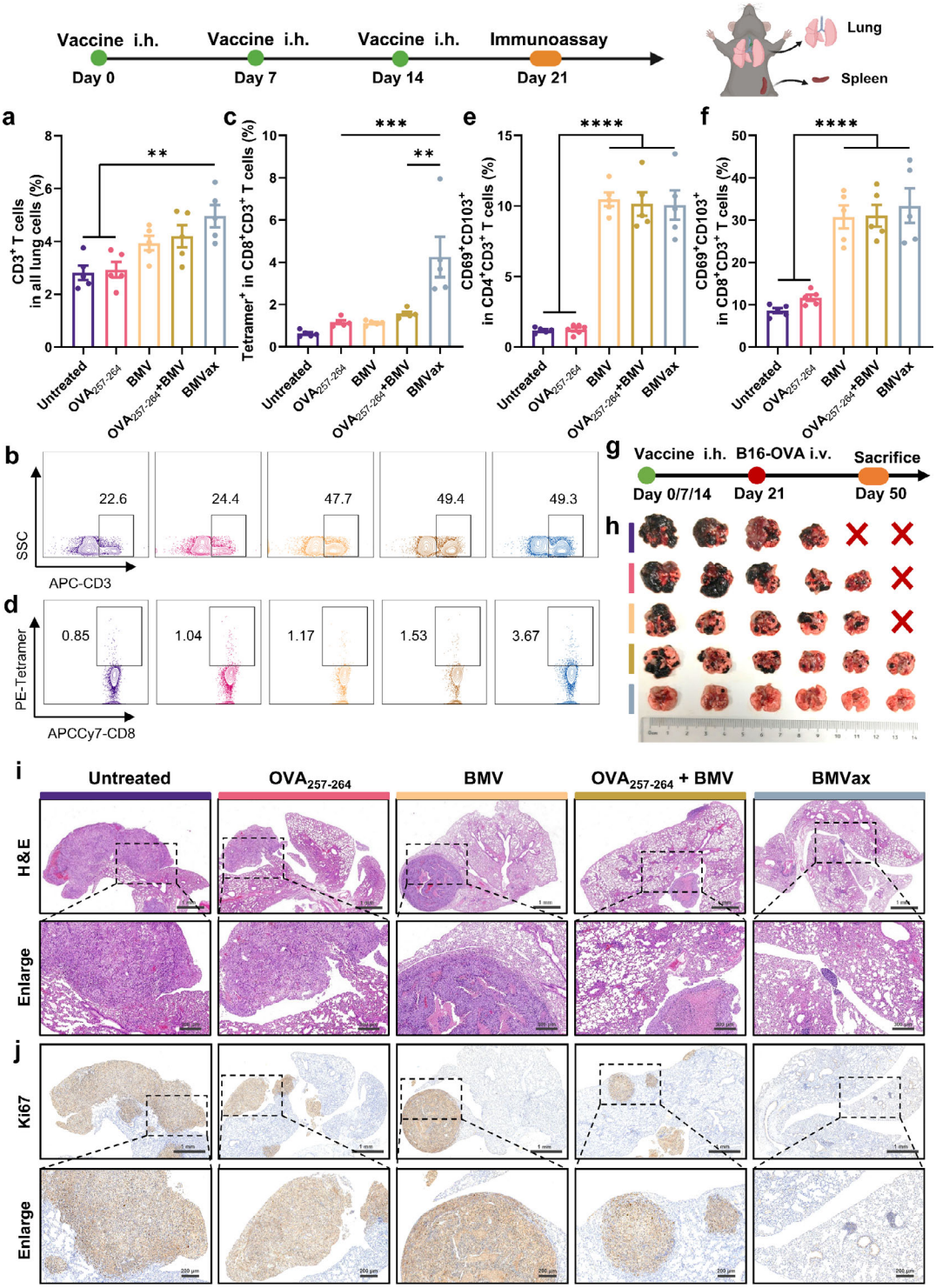

Figure 4. In vivo evaluation of immune responses and anti-metastatic efficacy of inhalable BMVax nanovaccine. a,b) Statistical data (a) showing the proportion of $CD3^+$ T cells within total lung cell populations and representative flow cytometry diagram (b) showing the proportion of $CD3^+$ T cells in lung single cell suspensions from mice with different treatments. c,d) Statistical data (c) and representative flow cytometry diagram (d) showing the proportion of $H2K^b$/SIINFEKL Tetramer$^+$ cells in $CD3^+CD8^+$ T cells in different groups. e,f) Statistical data showing the proliferation of $CD69^+CD103^+$ cells in $CD4^+CD3^+$ T cells (e) and $CD69^+CD103^+$ cells in $CD8^+CD3^+$ T cells (f). g) Timeline of the prophylactic cancer challenging experimental design. h) Photos of lungs collected from mice in different groups on day 50 ($n = 6$). i) Representative H&E staining of lung sections from mice in different groups. Scale bars:1 mm; enlarge: 300 μm. j) Representative Ki67 immunohistochemical staining demonstrating proliferative activity in lung tissues. Scale bars: 1 mm; enlarge: 200 μm). Data are presented as the mean ± SEM ($n = 5$). Statistical significance was calculated via one-way ANOVA in GraphPad Prism. * $p < 0.05$, ** $p < 0.01$, *** $p < 0.001$, and **** $p < 0.0001$.

analysis. As shown in Figure 4h, all groups except the BMVax-immunized group exhibited prominent tumor nodules in their lungs. Moreover, mice in the untreated, free antigen, and BMV groups succumbed to tumor burden during the experimental period. To quantify the anti-tumor effect, the weights of the lung in different groups were measured (Figure S25, Supporting Information). The results showed a significant increase in lung weight in some mice due to the higher tumor burden, whereas none of the BMVax immunized mice showed obvious lung metastases, and the lung weight remained at normal levels. Further histological analysis via hematoxylin and eosin (H&E) staining corroborated this observation, revealing an absence of metastatic foci in the lung tissues of BMVax-immunized mice (Figure 4i). To further evaluate tumor cell proliferation in lung metastases, we performed Ki67 immunohistochemical staining, as Ki67 serves as a recognized indicator of cellular proliferation and tumor aggressiveness. As shown in Figure 4j, the significantly reduced Ki67 expression in the BMVax-treated group underscores its effective capacity to suppress tumor proliferation in metastatic lung tissues. To further elucidate the immunological mechanisms driving BMVax-mediated protection, we conducted depletion experiments targeting $CD8^+$ T cells and B cells during the vaccination phase. As shown in Figure S26 (Supporting Information), the depletion of either $CD8^+$ T cells or B cells prior to BMVax administration markedly compromised the vaccine's protective efficacy against B16-OVA lung metastases. Notably, mice lacking $CD8^+$ T cells exhibited the most pronounced metastatic burden, while those with depleted B cells also developed enhanced lung tumor nodules. These findings indicate that both $CD8^+$ T cells and B cell-mediated responses contribute to the anti-tumor efficacy of BMVax, with $CD8^+$ T cells playing a predominant role. These results provide compelling evidence for the potential of BMVax as an effective strategy in lung metastatic cancer immunoprevention, further highlighting its promising role in combating tumor progression.

2.4. Therapeutic Effect of Inhalable BMVax Nanovaccine

Given the limitations of conventional subcutaneous immunization in eliciting strong local mucosal responses, the immune activation and prophylactic potential induced by inhaled BMVax suggest it as a promising alternative to the subcutaneous route. Therefore, the therapeutic efficacy of the inhalable BMVax nanovaccine was further assessed against traditional subcutaneous administration in treating established lung metastases. As shown in **Figure 5**a, C57BL/6 mice were intravenously inoculated with 1×10^6 B16-OVA cells on day 0. Following random group assignment, interventions began on day 5 and were administered weekly for three consecutive weeks. Groups included $OVA_{257\text{-}264}$ + BMV (direct lung delivery to simulate inhalation immunization: i.h.), BMVax (i.h.), and BMVax (subcutaneous immunization: s.c.), each receiving an equivalent $OVA_{257\text{-}264}$ dose of 10 μg per mouse and a consistent BMV protein concentration of 30 μg per mouse. To evaluate the therapeutic efficacy, mice were sacrificed on day 21, and TBLNs along with tumor-bearing lung tissues were collected for comprehensive analysis. Representative lung images (Figure S27, Supporting Information) revealed extensive melanoma lung metastases in the untreated group, while subcutaneous immunization exhibited a moderate therapeutic effect. In contrast, the inhalable BMVax group displayed the fewest visible metastatic lesions, underscoring its potent efficacy.

As a key site for pulmonary immune activation, the TBLNs exhibited a robust immune response following inhalable BMVax immunization, consistent with the effects observed during prophylactic immunization. Notably, GC B cells expanded two-fold compared to subcutaneous immunization (Figure 5b–e), and Tfh cells increased by 2.8-fold (Figure 5f,g), further highlighting the superior immunostimulatory capacity of the inhalable formulation. However, subcutaneous BMVax immunization failed to significantly enhance total T cells or antigen-specific T cells in the lung tissue compared to the untreated group (Figure 5h; Figures S30 and S31, Supporting Information), resulting in suboptimal therapeutic efficacy. In contrast, inhalable BMVax remarkably increased the accumulation of antigen-specific T cells in the lungs, reaching 14.8% (Figure 5i,j). Similar to the effect during prophylactic immunization, inhalable BMVax also significantly increased the presence of lung tissue-resident ($CD69^+CD103^+$) $CD4^+$ and $CD8^+$ T cells (Figure 5k,l; Figures S32 and S33, Supporting Information), reinforcing the localized immune protective effect. The levels were 2.2-fold and 2.9-fold higher than those observed in the subcutaneous immunization group, respectively. Within lung tumor lesions, all immunized groups exhibited tumor-infiltrating T cell responses (Figure 5m–p; Figure S35, Supporting Information). However, analysis of T cell proliferation and cytotoxic activity (Figure 5q,r; Figure S36, Supporting Information) revealed that only inhalable BMVax induced the highest intratumoral IFN-γ expression, which was 2.9-fold and 6.8-fold higher than that observed in the inhaled antigen + BMV mixture group and the subcutaneous BMVax group, respectively. These findings indicate that although subcutaneous BMVax immunization elicited a moderate cellular immune response and increased the proportion of tumor-infiltrating T cells, it failed to effectively activate the tracheobronchial lymph nodes or establish a robust tissue-resident immune response, resulting in limited tumor control. In contrast, inhalable BMVax not only induced potent B cell and Tfh cell immune responses but also promoted the expansion of antigen-specific T cells in the lungs, enhanced the cytotoxicity and proliferative capacity of tumor-infiltrating T cells, and ultimately conferred superior antitumor immunity. Consistent with these findings, the inhaled BMVax group demonstrated significantly prolonged survival compared to the subcutaneous and untreated groups (Figure 5s), further underscoring its therapeutic superiority.

3. Conclusion

In summary, we developed an innovative inhalable nanovaccine, BMVax, derived from genetically engineered *E. coli* expressing the ClyA-$OVA_{257\text{-}264}$ fusion protein. The extracted BMVax exhibited a uniform and stable nanoscale size, while effectively preserving the expression of the fusion protein. Proteomic analysis confirmed that its protein components predominantly originated from bacterial membrane fractions, ensuring the retention of intrinsic immunostimulatory properties, and enabling effective antigen co-delivery as a built-in adjuvant. In vitro studies demonstrated that BMVax significantly enhanced dendritic cell

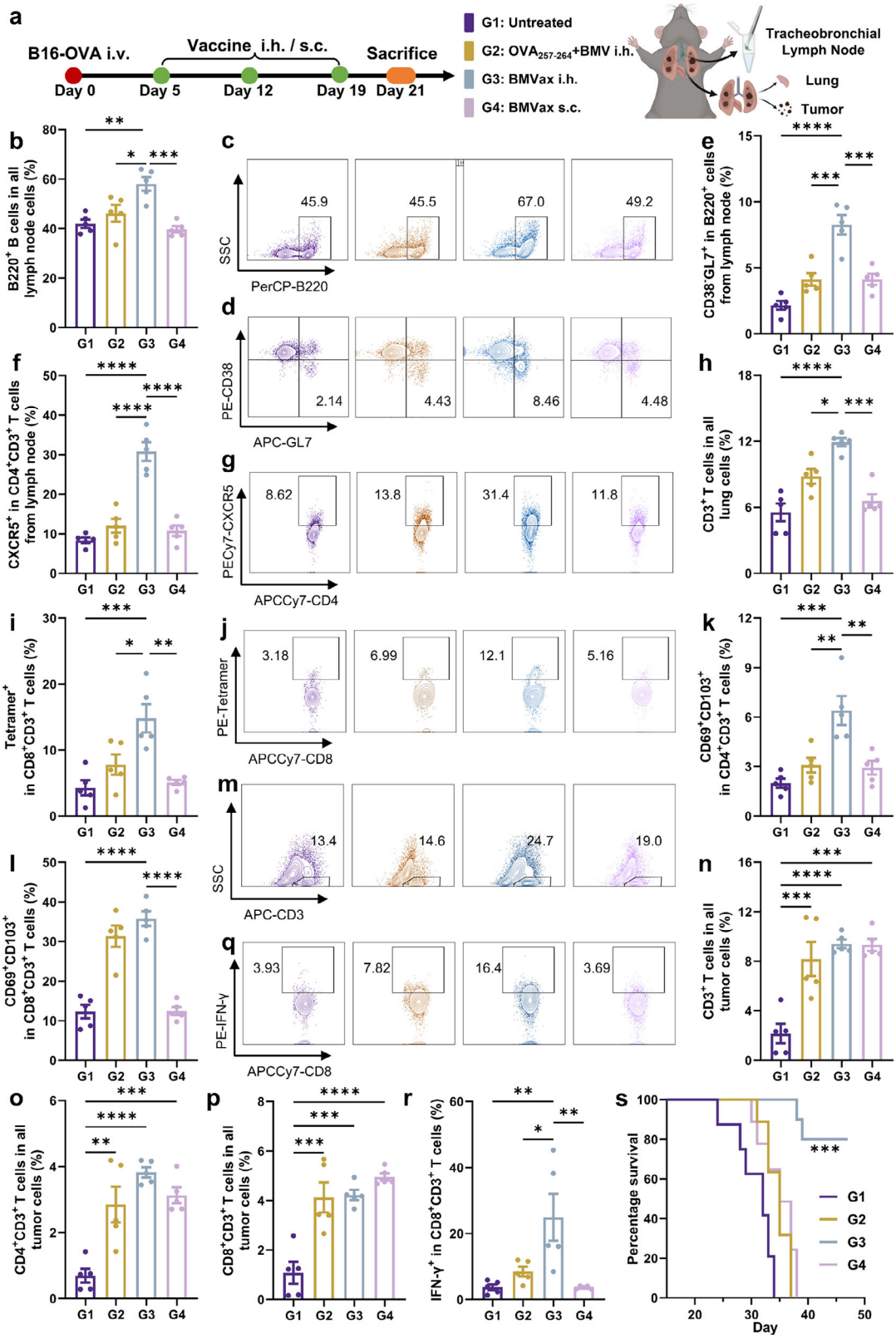

antigen uptake and facilitated efficient lysosomal escape, leading to a remarkable improvement in cross-presentation (2.2-fold increase compared to the antigen + BMV mixture group) and robust proliferation of antigen-specific T cells. In vivo, direct lung immunization with BMVax elicited potent immune responses in the tracheobronchial lymph nodes, resulting in a ≈5.8-fold and ≈4.9-fold increase in germinal center B cells and follicular helper T cells, respectively. Antigen-specific T-cell levels in lung tissues increased by 2.7-fold, and notably, only inhaled BMVax effectively induced systemic T-cell responses in the spleen. These findings indicate that BMVax can stimulate both local mucosal and systemic immunity, achieving an 83.3% complete prevention of lung metastases in immunized mice. Furthermore, in a therapeutic lung metastasis model, inhaled BMVax not only activated immune responses in the tracheobronchial lymph nodes but also promoted the recruitment of tissue-resident and antigen-specific T cells in the lungs, while enhancing the cytotoxicity and proliferation of tumor-infiltrating T cells. Notably, its therapeutic efficacy significantly surpassed that of subcutaneous immunization, which merely increased the number of tumor-infiltrating T cells without effectively activating immune responses in the lymph nodes or promoting antigen-specific T-cell recruitment in lung tissues. In conclusion, these results highlight the potential of inhalable BMVax as a next-generation vaccine platform for mucosal immunization and cancer immunotherapy, providing a compelling alternative to traditional subcutaneous injection strategies for the treatment of metastatic tumors. BMVax presents a promising alternative to conventional inhalable vaccine platforms such as live-attenuated, inactivated, subunit, or genetic vaccines, which often face challenges related to safety, suboptimal immunogenicity, or complex manufacturing processes. By integrating antigen delivery, immune stimulation, and scalable production into a single vesicle-based formulation, BMVax effectively addresses these limitations, highlighting the translational potential of BMVax for pulmonary vaccination.

4. Experimental Section

Materials: The model antigenic peptides $OVA_{257-264}$ (SIINFEKL) and FITC-$OVA_{257-264}$ were synthesized by GenScript. 3-(4,5-Dimethylthiazol-2-yl)-2,5-diphenyl tetrazolium bromide (MTT) and Lipopolysaccharide (LPS) were purchased from Sigma–Aldrich. Fluorescein isothiocyanate (FITC) was purchased from J&K (960900).

Cell Lines: DC2.4 cells (obtained from the American Type Culture Collection) and MLE12 cells (obtained from the American Type Culture Collection) were cultured in Roswell Park Memorial Institute (RPMI) 1640 medium (Pricella Life Science & Technology Co., Ltd., PM150110) containing 10% fetal bovine serum (FBS) (Inner Mongolia Jin Yuan Kang Biotechnology Co., Ltd., JYK-FBS-301) and 1% penicillin-streptomycin (Pricella Life Science & Technology Co., Ltd., PB180120) at 37 °C in 5% CO_2. B16-OVA cells (obtained from the American Type Culture Collection) were cultured in RPMI-1640 medium with 10% FBS and 1% penicillin-streptomycin, at 37 °C in 5% CO_2. Bone-marrow-derived dendritic cells (BMDCs) were isolated from C57BL/6 mice, and cultured in the complete DC medium containing 10% FBS, 1% penicillin- streptomycin, 55 µM β-mercaptoethanol (Gibco, 2466010), 20 ng mL^{-1} granulocyte-macrophage colony stimulating factor (GM-CSF, Novoprotein, Shanghai, China, CK02), and 10 ng mL^{-1} Interleukin-4 (IL-4, HUABIO, HA210902) at 37 °C with 5% CO_2. OT-I T cells were isolated from the spleens of female OT-I transgenic mice, and cultured in 1640 complete medium with 55 µM β-mercaptoethanol (Gibco, 2466010), 4 mM HEPES (Pricella Life Science & Technology Co., Ltd., PB180325), and 1 mM Sodium Pyruvate (Absin, abs44076143) at 37 °C in 5% CO_2.

Animals: Female C57BL/6 mice (6–8 weeks) were purchased from Changzhou Cavens Experimental Animal Co Ltd. Female OT-I transgenic mice (6–8 weeks) were a gift from Prof. Z. Liu (Soochow University). All animal experiments were performed in compliance with the relevant laws and approved by the Institutional Animal Care and Use Committee of Soochow University (No. SUDA20240724A01). The mice were housed in an environmentally controlled room (23 °C, 55 ± 5% humidity, with a 12 h:12 h light: dark cycle). The mice in operation were anesthetized through intraperitoneal injection with 0.5% pentobarbital (0.1 mL per 10 g of body weight).

Construction of Engineered Bacteria E. Coli-$OVA_{257-264}$: *Escherichia coli* (*E. coli*, strain TOP10) was purchased from the American Type Culture Collection (ATCC). The pBAD-ClyA-OVA plasmid was constructed using restriction enzyme-mediated integration (REMI) according to a previously published protocol. The ClyA-$OVA_{257-264}$ sequence was codon-optimized to enhance expression in *E. coli*, and the optimized sequence was inserted into the pBAD His A vector at NcoI and HindIII restriction sites. The pBAD-ClyA-OVA plasmid was subsequently introduced into *E. coli* (*E. coli*-$OVA_{257-264}$) via electroporation. The transformed strains were then cultured at 37 °C in lysogeny broth (LB) containing 100 µg mL^{-1} ampicillin, with shaking at 180 rpm.

Preparation and Characterization of BMVs: *E. coli* and *E. coli*-$OVA_{257-264}$ were harvested into centrifuge tubes and centrifuged at 6000 rpm for 30 min at 4 °C. The bacterial pellets were washed twice with 1×PBS to remove residual medium, followed by resuspension in sterile double-distilled water (dd H_2O). Bacterial disruption was performed using a Sonic Disruptor for 1 h on ice (sonication cycle: Ton = 3 s, Toff = 5 s, ultrasonic power = 300 W). The resulting lysate underwent three cycles of freeze-thaw using liquid nitrogen and a 37 °C-water bath to ensure complete disruption of the cells. The suspension was then centrifuged at 6000 rpm for 30 min at 4 °C to remove intact cells and large debris, and the supernatant was collected. Further purification was performed by ultracentrifugation at 14 800 rpm for 30 min at 4 °C, and the resulting pellet was resuspended in sterile PBS. Finally, the protein concentration was

Figure 5. Therapeutic effect of inhalable BMVax nanovaccine against lung metastasis. a) Experimental timeline detailing the treatment of BMVax nanovaccine against lung metastases. b,c) Statistical data (b) showing the proportion of $B220^+$ B cells within total lymph node cell populations from mice with different treatments and representative flow cytometry diagram (c) showing the proportion of $B220^+$ B cells from the lymphocyte population (based on FSC/SSC) after debris exclusion and a de-adhesion step in lymph node single cell suspensions. d,e) Representative flow cytometry diagram (d) and statistical analysis (e) showing the proportion of $CD38^-GL7^+$ cells in $B220^+$ cells. f,g) Statistical data (f) and representative flow cytometry diagram (g) showing the proportion of $CXCR5^+$ cells in $CD4^+CD3^+$ T cells. h) Statistical data showing the proportion of $CD3^+$ T cells among total lung single-cell suspensions from mice with different treatments. i,j) Statistical data (i) and representative flow cytometry diagram (j) showing the proportion of $Tetramer^+$ cells in $CD8^+CD3^+$ T cells in lung tissues. k,l) Statistical data showing the proliferation of $CD69^+CD103^+$ cells in $CD4^+CD3^+$ T cells (k) and $CD69^+CD103^+$ cells in $CD8^+CD3^+$ T cells (l). m,n) Representative flow cytometry diagram (m) showing the proportion of $CD3^+$ T cells from the lymphocyte population (based on FSC/SSC) after debris exclusion and a de-adhesion step in tumor single cell suspensions from mice with different treatments and statistical data (n) showing the proportion of $CD3^+$ T cells within total tumor cell populations. o,p) Statistical data showing the proportion of $CD4^+CD3^+$ and $CD8^+CD3^+$ cells within total tumor cell populations. q,r) Representative flow cytometry diagram (q) and statistical data (r) showing the proportion of IFN-γ^+ T cells in $CD8^+CD3^+$ T cells. s) Survival profiles of the mice bearing B16-OVA lung metastasis model with different treatments ($n = 6$). Other data are presented as the mean ± SEM ($n = 5$). Statistical significance was calculated via one-way ANOVA, and the survival curve was calculated via the Kaplan-Meier method in GraphPad Prism. * $p < 0.05$, ** $p < 0.01$, *** $p < 0.001$, and **** $p < 0.0001$.

determined using a bicinchoninic acid (BCA) protein assay kit (Beijing Boxbio Science & Technology Co., Ltd., AKPR017). The samples were aliquoted and stored at −80 °C for future use or lyophilized with 5% trehalose and stored at 4 °C. The sizes and zeta potentials of obtained BMV and BMVax were measured by a Zetasizer Nano ZS (Malvern Instruments). The morphology of BMV and BMVax was observed using an FEI Tecnai G2 F20 Transmission Electron Microscope (TEM). To investigate the stability of the nanovaccine, BMV and BMVax were dispersed in 1×PBS at physiological temperature (37 °C), and their sizes and polydispersity index (PDI) were monitored over time. The endotoxin levels in BMV and BMVax were determined using a LAL-based endotoxin detection kit (Beyotime, C0276S).

Western Blotting Analysis: To verify the expression of the fusion protein, bacteria subjected to different treatments were collected and processed through centrifugation, washing, ultrasonic disruption, and repeated freeze-thaw cycles. A portion of the sample was used to extract BMVs as previously described. The total protein content from bacteria under different treatments, as well as the corresponding BMVs, was quantified using the BCA protein assay. Protein samples were separated using 10% sodium dodecyl sulfate-polyacrylamide (SDS-PAGE) gels along with a pre-stained protein marker (Shanghai EpizymeV, Shanghai, China, WJ103) and subsequently transferred onto a polyvinylidene fluoride (PVDF) membrane (Shandong Sparkjade Biotechnology Co., Ltd., ED0004). Membranes were blocked with 5% BSA for 1 h at room temperature and incubated overnight at 4 °C with primary anti-HA tag antibody (1:5000, Proteintech, 51064-2-AP). After washing with Tris Buffered Saline containing 0.1% Tween 20 (TBST) three times, membranes were incubated with HRP-conjugated Goat Anti-Rabbit IgG (H+L) Antibody (APExBIO, Houston, USA, K1223) for 2 h at room temperature. Finally, membranes were washed thrice with TBST, incubated with ECL reagent (Shandong Sparkjade Biotechnology Co., Ltd., ED0016), and imaged by the Amersham Imager 600 System (General Electric Company, USA). DC2.4 cells were seeded in 6-well plates at a density of 1×10^6 cells per well. Following overnight incubation, cells were incubated with BMVax (5 μg mL^{-1}) and $OVA_{257\text{-}264}$ (5 μg mL^{-1}) at 37 °C for 12 h. Then, the cells were lysed by Western and IP Cell lysis Buffer (Beyotime, P0013) containing 0.1% protease inhibitor (Sigma–Aldrich, P8340) and 0.1% phosphatase inhibitor (Sigma–Aldrich, P2850) at 4 °C for 30 min. The lysates were collected, centrifuged, and the protein concentration was measured by a BCA protein assay kit (Beijing Boxbio Science & Technology Co., Ltd., AKPR017). Protein samples were separated using 10% SDS-PAGE gels with a pre-stained protein marker (Shanghai EpizymeV, Shanghai, China, WJ103) and transferred onto a PVDF membrane (Shandong Sparkjade Biotechnology Co., Ltd., ED0004). Membranes were blocked with 5% BSA for 1 h at room temperature and incubated overnight at 4 °C with primary antibodies, including anti-GAPDH (1:10000, Abcam, AB181602), anti-NF-κB p65 (1:1000, Abcam, AB76302), and anti-TLR4 (1:1000, Proteintech, 30400-1-AP). After washing with TBST three times, membranes were incubated with HRP Goat Anti-Rabbit IgG (H+L) Antibody (APExBIO, Houston, USA, K1223) for 2 h at room temperature. Finally, membranes were washed thrice with TBST, incubated with ECL reagent (New Cell & Molecular Biotech, P10200), and imaged by the Amersham Imager 600 System (General Electric Company, USA).

Cellular Uptake and Staining: DC2.4 cells were seeded in 24-well plates at a density of 5×10^5 cells per well. Following overnight incubation, the cells were treated with FITC-$OVA_{257\text{-}264}$ (5 μg mL^{-1}) or FITC-BMVax (5 μg mL^{-1}), ensuring consistent FITC fluorescence intensity, for 6 h. Then, the uptake of FITC by cells in different groups was analyzed by flow cytometry. For the internalization assay, DC2.4 cells were cultured in confocal dishes (NEST Biotechnology, 801001) and incubated with FITC-$OVA_{257\text{-}264}$ (5 μg mL^{-1}) or FITC-BMVax (5 μg mL^{-1}) for 6 h. Following incubation, cells were washed three times with PBS, fixed with 4% paraformaldehyde (15 min, RT), and stained with DAPI (1 μg mL^{-1}, 10 min) for nuclear visualization. Cellular images were acquired using a fluorescence microscopy (Leica DMi8, 20× objective). To analyze cellular localization, DC2.4 cells were cultured in glass dishes (NEST Biotechnology, 801001) and incubated with FITC-$OVA_{257\text{-}264}$ (5 μg mL^{-1}) or FITC-BMVax (5 μg mL^{-1}) for 4 and 8 h. Following incubation, cells were washed three times with PBS to remove unbound particles, then stained with Hoechst (7.5 μg mL^{-1}, 10 min) and LysoTracker Red (100 nM, 30 min). Imaging was performed using a confocal laser scanning microscope (ZEISS LSM 800 with Airyscan). For confocal imaging, samples were examined with a 40× objective lens. Excitation settings were: 405 nm laser at 3.5% power for Hoechst (master gain 770 V), 488 nm at 4.5% for FITC (700 V), and 561 nm at 3.5% for LysoTracker Red (720 V). All images were acquired under identical settings to ensure consistent comparative analysis. To evaluate antigen presentation efficiency, DC2.4 cells were cultured in confocal dishes (NEST Biotechnology, 801001) and incubated with BMVax (5 μg mL^{-1}) and $OVA_{257\text{-}264}$ (5 μg mL^{-1}) for 24 h. Cells were then washed three times with PBS, fixed with 4% paraformaldehyde (15 min, RT), and stained with the following markers: DAPI (1 μg mL^{-1}, 10 min) for nuclei, AlexaFluor 488 phalloidin (1:100 dilution, 20 min) for actin cytoskeleton, and APC-anti-SIINFEKL-$H2K^b$ antibody (BioLegend, 141606; 1:500, 1 h) for MHC-I antigen presentation. Cellular imaging was performed using a fluorescence microscopy (Leica DMi8, 20× objective).

In Vivo Immune Responses: After different treatments, the mice were sacrificed, and their TBLNs were collected and placed in Fluorescence-Activated Cell Sorting buffer (FACS buffer) — 1×PBS (Bioland, FL10210) + 2% FBS (Cellmax, SA301.03.V, Beijing). The lymph nodes were then mechanically processed to generate a single-cell suspension. Then, the cells were first incubated with anti-CD16/32 (BioLegend, 101303) at room temperature to block non-specific binding sites. Subsequently, the cells were labeled with a panel of antibodies: FITC-anti-B220 (BioLegend, 103206), APC-anti-GL7 (BioLegend, 144617), PE/Cy7-anti-CD95 (BioLegend, 152617), PE-anti-CD38 (BioLegend, 102708); FITC-anti-CD11c (BioLegend, 117306), PE/Cy7-anti-CD80 (BioLegend, 104734), APC/Cy7-anti-CD86 (BioLegend, 105014), APC-anti-$H2K^b$ bound to SIINFEKL (BioLegend, 141606); FITC-anti-CD3 (BioLegend, 100204), PE/Cy7-anti-CD4 (BioLegend, 100422), APC-anti-PD1 (BioLegend, 143710), PE-anti-CXCR5 (BioLegend, 145503), APC/Cy7-anti-ICOS (BioLegend, 313529) for flow cytometry analysis (Fongcyte). To investigate antigen-specific T cell activation in the lung, lung tissues from immunized mice were isolated and mechanically disrupted. Lung single-cell suspensions were isolated by lymphocyte isolation fluid (Dakewe Biotech, 7211011) and the Lymphocyte Separation Tube (NEST Biotechnology, 601852). Then, splenocytes were blocked with anti-CD16/32 (BioLegend, 101303) at room temperature. The cells were subsequently stained with APC-anti-CD3 (BioLegend, 100236), APC/Cy7-anti-CD8 (BioLegend, 100714), and PE/Cy7-anti-CD4 (BioLegend, 100422), PerCP-anti-CD103 (BioLegend, 121416), FITC-anti-CD69 (BioLegend, 104506), and PE-labeled SIINFEKL-MHC-I tetramer for flow cytometry analysis (Fongcyte). To explore the systemic cellular immune response, the spleens were then mechanically processed to generate a single-cell suspension and lysed for erythrocytes (ZUNYAN, NanJing, China, ZYFB006-0100). Splenocytes collected from immunized mice were incubated with $OVA_{257\text{-}264}$ peptide (Invivogen, 10 μg mL^{-1}) and PMA + Ionomycin (Dakewe Biotech, 2030421) in the presence of Brefeldin A (Adamas-life, Y35485), an inhibitor for protein transport, for 6 h. Then, the cells were stained with FITC-anti-CD3 (BioLegend, 100204), PerCP-anti-CD8 (BioLegend, 100732), APC/Cy7-anti-CD4 (BioLegend, 100414), APC-anti-IFN-γ (BioLegend, 505810), PE-anti-TNF-α (BioLegend, 506306), and PE-labeled SIINFEKL-MHC-I tetramer for flow cytometry analysis (Fongcyte).

Statistical Analysis: All the values in the present study are presented as the mean ± SEM unless otherwise indicated in the figure captions. Ordinary one-way ANOVA was used for multiple comparisons (when more than two groups were compared), and an unpaired *t*-test was used for two-group comparisons. Survival curve was calculated via the Kaplan-Meier method and compared by the log-rank test. All statistical analyses were carried out with the GraphPad Prism software package (PRISM 10.1.2; GraphPad Prism Software) or Excel 2016. The threshold for statistical significance was $^{*}p < 0.05$, $^{**}p < 0.01$, $^{***}p < 0.001$, and $^{****}p < 0.0001$. All figure illustrations were created with BioRender.com.

Supporting Information

Supporting Information is available from the Wiley Online Library or from the author.

Acknowledgements

Y.M. and H.Z. contributed equally to this work. This article was partially supported by the National Research Programs of China (2020YFA0211100, 2022YFA1206500), the National Natural Science Foundation of China (52450010, 52325106, 52271248), Natural Science Foundation of Jiangsu Province (BK20240040), the Collaborative Innovation Center of Suzhou Nano Science and Technology, the Suzhou Key Laboratory of Nanotechnology and Biomedicine and the 111 Program from the Ministry of Education of China.

Conflict of Interest

The authors declare no conflict of interest.

Data Availability Statement

The data that support the findings of this study are available from the corresponding author upon reasonable request.

Keywords

cancer immunotherapy, genetically engineered bacteria, inhalable nanovaccine, lung metastasis, membrane vesicles

Received: April 1, 2025
Revised: July 16, 2025
Published online:

[1] F. Martínez-Jiménez, A. Movasati, S. R. Brunner, L. Nguyen, P. Priestley, E. Cuppen, A. Van Hoeck, *Nature* **2023**, *618*, 333.
[2] N. K. Altorki, G. J. Markowitz, D. Gao, J. L. Port, A. Saxena, B. Stiles, T. McGraw, V. Mittal, *Nat. Rev. Cancer* **2019**, *19*, 9.
[3] X. Zhai, L. Yang, S. Chen, Q. Zheng, Z. Wang, *Cancer Med.* **2016**, *5*, 2286.
[4] S. Karim, S. Nanji, K. Brennan, C. Pramesh, C. M. Booth, *Eur. J. Surg. Oncol. (EJSO)* **2017**, *43*, 236.
[5] C. Springfeld, C. R. Ferrone, M. H. G. Katz, P. A. Philip, T. S. Hong, T. Hackert, M. W. Büchler, J. Neoptolemos, *Nat. Rev. Clin. Oncol.* **2023**, *20*, 318.
[6] A. Shinde, R. Li, A. Amini, S. Glaser, *J. Clin. Oncol.* **2019**, *37*, 1030.
[7] Q. Zhan, B. Liu, X. Situ, Y. Luo, T. Fu, Y. Wang, Z. Xie, L. Ren, Y. Zhu, W. He, Z. Ke, *Signal Transduction Targeted Ther.* **2023**, *8*, 465.
[8] L. Chen, J. Shen, Z. Kang, Z. Zhang, Z. Zheng, L. Zhang, Z. Xiao, Q. Zhang, H. Fang, J. Zhou, Y. Wang, Y. Yang, Z. Liu, Q. Chen, *Chem* **2024**, *10*, 1783.
[9] P. A. Kiberstis, *Science* **2018**, *359*, 1373.
[10] M. Graciotti, L. E. Kandalaft, *Nat. Rev. Drug Discovery* **2025**, *24*, 134.
[11] M. Saxena, S. H. van der Burg, C. J. Melief, N. Bhardwaj, *Nat. Rev. Cancer* **2021**, *21*, 360.
[12] L. Niu, Y. Miao, Z. Cao, T. Wei, J. Zhu, M. Li, B. Bai, L. Chen, N. Liu, F. Pan, J. Zhu, C. Wang, Y. Yang, Q. Chen, *ACS Nano* **2024**, *18*, 3349.
[13] Z. Kang, L. Chen, P. Li, Z. Zheng, J. Shen, Z. Xiao, Y. Miao, Y. Yang, Q. Chen, *Sci. Adv.* **2025**, *11*, adt0341.
[14] Z. Cao, L. Ren, L. Niu, R. Zhao, N. Liu, Q. Zhuang, F. Pan, Z. Liu, Y. Cheng, Y. Yang, Q. Chen, *Matter* **2023**, *6*, 3574.
[15] J. H. Buckner, *Nat. Rev. Rheumatology* **2025**, *21*, 88.
[16] Y. Miao, L. Niu, X. Lv, Q. Zhang, Z. Xiao, Z. Ji, L. Chen, Y.i Liu, N. Liu, J. Zhu, Y. Yang, Q. Chen, *Adv. Mater.* **2024**, *36*, 2410715.
[17] Z. Xiao, G. Li, D. Deng, T. Wei, G. Chen, H. Tao, Y.u Chao, B.o Liu, Q. Li, Y. Yang, Z. Liu, Q. Chen, *Adv. Funct. Mater.* **2023**, *34*, 2314022.
[18] P. Zhang, J. Meng, Y. Li, C. Yang, Y. Hou, W. Tang, K. J. McHugh, L. Jing, *Innovation* **2021**, *2*, 100174.
[19] A. Mantovani, F. Marchesi, D. Di Mitri, C. Garlanda, *Cell Mol. Immunol.* **2024**, *21*, 1201.
[20] E. C. Lavelle, R. W. Ward, *Nat. Rev. Immunol.* **2022**, *22*, 236.
[21] X. Zhou, Y. Wu, Z. Zhu, C. Lu, C. Zhang, L. Zeng, F. Xie, L. Zhang, F. Zhou, *Signal Transduction Targeted Ther.* **2025**, *10*, 7.
[22] Z. Wang, K. D. Popowski, D. Zhu, B. L. de Juan Abad, X. Wang, M. Liu, H. Lutz, N. De Naeyer, C. T. DeMarco, T. N. Denny, P.-U. C. Dinh, Z. Li, K. Cheng, *Nat. Biomed. Eng.* **2022**, *6*, 791.
[23] T. Ye, Z. Jiao, X. Li, Z. He, Y. Li, F. Yang, X. Zhao, Y. Wang, W. Huang, M. Qin, Y. Feng, Y. Qiu, W. Yang, L. Hu, Y. Hu, Y. Zhai, E. Wang, D. Yu, S. Wang, H. Yue, Y. Wang, H. Wang, L. Zhu, G. Ma, W. Wei, *Nature* **2023**, *624*, 630.
[24] Y. Chen, S. Lin, L.u Wang, Y. Zhang, H. Chen, Z. Fu, M. Zhang, H. Luo, J. Liu, *Nat. Biomed. Eng.* **2024**, *8*, 823.
[25] L. Chen, R. Zhao, J. Shen, N. Liu, Z. Zheng, Y. Miao, J. Zhu, L. Zhang, Y. Wang, H. Fang, J. Zhou, M. Li, Y. Yang, Z. Liu, Q. Chen, *Adv. Mater.* **2023**, *35*, 2306281.
[26] Y. Dong, T. Dai, B. Wang, L. Zhang, L.-H. Zeng, J. Huang, H. Yan, L. Zhang, F. Zhou, *Signal Transduction Targeted Ther.* **2021**, *6*, 387.
[27] N. Krishnan, L. J. Kubiatowicz, M. Holay, J. Zhou, R. H. Fang, L. Zhang, *Adv. Drug Delivery Rev.* **2022**, *185*, 114294.
[28] A. Redenti, J. Im, B. Redenti, F. Li, M. Rouanne, Z. Sheng, W. Sun, C. R. Gurbatri, S. Huang, M. Komaranchath, Y. Jang, J. Hahn, E. R. Ballister, R. L. Vincent, A. Vardoshivilli, T. Danino, N. Arpaia, *Nature* **2024**, *635*, 453.
[29] L. Chen, Z. Kang, J. Shen, R. Zhao, Y. Miao, L. Zhang, Z. Zheng, Z. Zhang, N. Liu, C. Wang, H. Fang, J. Zhou, Y. Wang, Z. Liu, Y. Yang, Q. Chen, *Sci. Bull.* **2024**, *69*, 2565.
[30] M. Li, N. Liu, J. Zhu, Y. Wu, L. Niu, Y. Liu, L. Chen, B. Bai, Y. Miao, Y. Yang, Q. Chen, *Biomaterials* **2024**, *309*, 122584.
[31] C. Wang, L. Chen, J. Zhu, C. Wang, M. Li, Y. Miao, N. Liu, Z. Ji, F. Pan, Y. Liu, J. Zhu, Y. Yang, Q. Chen, *Adv. Funct. Mater.* **2024**, *34*, 2316092.
[32] J. Li, H. Zeng, L. Li, Q. Yang, L. He, M. Dong, *ACS Nano* **2023**, *17*, 24593.
[33] J. Shen, L. Chen, X. Lv, N. Liu, Y. Miao, Q. Zhang, Z. Xiao, M. Li, Y. Yang, Z. Liu, Q. Chen, *Adv. Mater.* **2024**, *36*, 2314095.
[34] M. Toyofuku, N. Nomura, L. Eberl, *Nat. Rev. Microbiol.* **2019**, *17*, 13.
[35] R. Richter, M. A. M. Kamal, M. Koch, B.-J. Niebuur, A.-L. Huber, A. Goes, C. Volz, J. Vergalli, T. Kraus, R. Müller, N. Schneider-Daum, G. Fuhrmann, J.-M. Pagès, C.-M. Lehr, *Adv. Healthcare Mater.* **2022**, *11*, 2101180.
[36] M. Toyofuku, S. Schild, M. Kaparakis-Liaskos, L. Eberl, *Nat. Rev. Microbiol.* **2023**, *21*, 415.
[37] Y. Li, X. Ma, Y. Yue, K. Zhang, K. Cheng, Q. Feng, N. Ma, J. Liang, T. Zhang, L. Zhang, Z. Chen, X. Wang, L. Ren, X. Zhao, G. Nie, *Adv. Mater.* **2022**, *34*, 2109984.
[38] S. Li, Y. Yue, W. Wang, M. Han, X. Wan, Q. Li, X. Chen, J. Cao, Y. Zhang, J. Li, J. Li, L. Cheng, J. Yang, D. Wang, Z. Zhou, *Adv. Mater.* **2024**, *36*, 2405953.
[39] T. M. Fenton, P. B. Jørgensen, K. Niss, S. J. S. Rubin, U. M. Mörbe, L. B. Riis, C. Da Silva, A. Plumb, J. Vandamme, H. L. Jakobsen, S. Brunak, A. Habtezion, O. H. Nielsen, B. Johansson-Lindbom, W. W. Agace, *Immunity* **2020**, *52*, 557.

[40] K. Rakhra, W. Abraham, C. Wang, K. D. Moynihan, N. Li, N. Donahue, A. D. Baldeon, D. J. Irvine, *Sci. Immunol.* **2021**, *6*, abd8003.
[41] C. R. Nowosad, K. M. Spillane, P. Tolar, *Nat. Immunol.* **2016**, *17*, 870.
[42] A. Martínez-Riaño, S. Wang, S. Boeing, S. Minoughan, A. Casal, K. M. Spillane, B. Ludewig, P. Tolar, *Nat. Immunol.* **2023**, *24*, 1281.
[43] W. S. Foster, J. L. Lee, N. Thakur, J. Newman, A. J. Spencer, S. Davies, D. Woods, L. Godfrey, I. M. Hay, S. Innocentin, J. C. Yam-Puc, E. C. Horner, H. J. Sharpe, J. E. Thaventhiran, D. Bailey, T. Lambe, M. A. Linterman, *Cell Rep. Med.* **2022**, *3*, 100845.
[44] F. Zhu, R. J. McMonigle, A. R. Schroeder, X. Xia, D. Figge, B. D. Greer, E. González-Avalos, D. O. Sialer, Y.-H. Wang, K. M. Chandler, A. J. Getzler, E. R. Brown, C. Xiao, O. Kutsch, Y. Harada, M. E. Pipkin, H. Hu, *Nat. Commun.* **2023**, *14*, 3611.
[45] Z. Xiao, A. T. Mayer, T. W. Nobashi, S. S. Gambhir, *Cancer Res.* **2020**, *80*, 3023.
[46] S. Houston, *Nat. Immunol.* **2023**, *24*, 1781.
[47] A. Das, B. A. Heesters, A. Bialas, J. O'Flynn, I. R. Rifkin, J. Ochando, N. Mittereder, G. Carlesso, R. Herbst, M. C. Carroll, *Immunity* **2017**, *46*, 106.
[48] A. Kaminski, F. T. Hager, L. Kopplin, F. Ticconi, A. Leufgen, E. Vendelova, L. Rüttger, G. Gasteiger, V. Cerovic, W. Kastenmüller, O. Pabst, M. Ugur, *Sci. Immunol.* **2023**, *8*, adj5789.